Separation and Purification Technology 391 (2026) 137148

Contents lists available at ScienceDirect

Separation and Purification Technology

journal homepage: www.elsevier.com/locate/seppur

Selective Lithium extraction from clay minerals using a Superacidic urea–Methanesulfonic acid deep eutectic solvent

Hosein Ghaedi [a,*], Cristian Serrano Araya [a,e], Payam Kalhor [b], Cora Dawson-Jones [a], Enrico Ferrari [c], Tasnim Munshi [d], Ian Scowen [a], Yousef Ghorbani [a,*]

[a] College of Health and Science, School of Natural Sciences, Department of Chemistry, Joseph Banks Laboratories, University of Lincoln, Green Lane, Lincoln, Lincolnshire LN6 7DL, United Kingdom
[b] School of Chemistry, University of Southampton, Southampton SO17 1BJ, United Kingdom
[c] College of Health and Science, School of Natural Sciences, Department of Life Science, Joseph Banks Laboratories, University of Lincoln, Green Lane, Lincoln, Lincolnshire LN6 7DL, United Kingdom
[d] School of Chemical and Physical Sciences, Keele University, Staffordshire ST5 5BG, United Kingdom
[e] Department of Metallurgical and Mining Engineering, Universidad Católica del Norte, Av. Angamos 0610, Antofagasta, Chile

ARTICLE INFO

Keywords:
Methanesulfonic acid (MSA)
Deep eutectic solvent (DES)
Spectroscopic characterization
DFT
Acidity
Clay mineral
Metal extraction

ABSTRACT

Urea–methanesulfonic acid (MSA) deep eutectic solvents (DESs) are reported here for the first time as a green, superacidic platform for the highly selective extraction of lithium (Li) from clay-bearing ores. Formulated in molar ratios from 1:2 to 1:8, these DESs were characterized using Fourier-transform infrared spectroscopy (FTIR), Raman spectroscopy, ^{1}H and ^{13}C nuclear magnetic resonance (NMR), ultraviolet-visible (UV–Vis) spectroscopy, alongside density functional theory (DFT) to map their unique molecular interactions and tuneable acidity. Spectroscopic and computational analyses revealed a transition from hydrogen-bond-dominant to ionic environments as the MSA ratio increased, with DFT indicating rising interaction energies (1.583 to 3.237 eV) and vibrational signatures of protonation. The urea-MSA 1:2 system, optimized with 20% water, maintained superacidity ($H_0 = -3.102$) and achieved a remarkable 100% extraction efficiency for Li, Na, and Sr. Critically, the system exhibited superior selectivity, recovering 100% Li while leaching only 23% Al and 6% K, significantly outperforming conventional sulfuric acid (4% Li) and citric acid (92% Li). This selectivity is attributed to a "coordination window" where the superacidic protons effectively disrupt the mineral lattice while the DES components inhibit the total dissolution of structural impurities. These findings demonstrate that urea-MSA DESs serve as high-performance, recyclable, and sustainable alternatives for the selective recovery of critical metals. By operating at moderate temperatures with high atom economy, this system offers a viable industrial pathway for the green valorization of complex mineral matrices, addressing the urgent need for sustainable lithium sourcing in the global energy transition.

1. Introduction

The secure and sustainable primary source of lithium (Li) now constitutes an essential challenge to achieve the transition of the whole world to a low-carbon energy paradigm in view of its ever-increasing consumption by Li-ion batteries in electric transportation and portable electronics [1,2]. Although hard-rock pegmatites and salar brines have dominated historical Li production, sedimentary and clay-hosted deposits of Li are believed to have one of the largest yet unconsumed global Li reservoirs. Low grades, complicated mineralogy, and strong Li binding within aluminosilicate and clay matrices continue to significantly limit the economic exploitation of these deposits, despite their strategic advantages in terms of regional diversity and long-term supply security [3,4]. The common methods for Li clays involve the selective extraction of Li using inorganic acids such as sulfuric and hydrochloric acid, and in some cases, high-temperature roasting. These methods, although useful in some cases, involve high energy requirements, high concentration reagent use, and considerable environmental problems linked to the use and storage of the inorganic acids, as well as greenhouse gas (GHG) emissions, and several impurities in the solution [4–12]. Some studies have adopted the use of citric and oxalic acids as safer environments for Li extraction, but the low Li-extraction abilities and performance in the

* Corresponding authors.
E-mail addresses: hghaedi@lincoln.ac.uk (H. Ghaedi), YGhorbani@lincoln.ac.uk (Y. Ghorbani).

https://doi.org/10.1016/j.seppur.2026.137148
Received 27 December 2025; Received in revised form 30 January 2026; Accepted 2 February 2026
Available online 3 February 2026

extraction of Li structurally entrenched in clays make the quest for a better Li-extraction medium an absolute necessity. Deep eutectic solvents (DESs) have emerged over the past decade as a versatile class of designer solvents with tuneable physicochemical properties, formed through hydrogen-bonding interactions between hydrogen-bond donors (HBD) and acceptors (HBA) [13–15]. DESs have attracted growing attention in hydrometallurgy due to their low vapor pressure, chemical tunability, and potential for selective metal dissolution. To date, most DES research has focused on metal recovery from secondary resources [16–18], while their application to primary Li resources, particularly clay-hosted systems, remains comparatively underexplored. In addition, most DESs reported thus far can function within moderate acidity regimes, making them highly ineffective at breaking strong metal-oxygen bonds in aluminosilicate lattices. MSA is a strong acid, biodegradable, and represents an industrially established commodity that has potential advantages over classical mineral acids in terms of its high metal salt solubility, negligible vapor pressure, and satisfactory environmental profile [12,19–21]. When combined with appropriate HBDs such as urea, MSA has the potential to form deep eutectic systems capable of transitioning from hydrogen-bond-dominated networks to highly ionic, superacidic media. However, the fundamental structural evolution, acidity modulation, and metal-extraction behavior of urea–MSA systems across wide compositional ranges have not yet been systematically investigated.

The urea–MSA system reported here introduces a unique platform characterized by tunable superacidity. Unlike conventional DESs based on organic carboxylic acids, this system enables a controlled transition from hydrogen-bonded networks to highly reactive ionic environments. By modulating the molar ratio, the solvent achieves a superacidic state necessary for breaking strong metal-oxygen bonds in recalcitrant clay minerals. This creates an optimal 'coordination window' where superacidic protons disrupt the mineral lattice while urea components maintain the capacity to coordinate target metals, providing a level of selectivity against structural impurities like Al and K that traditional mineral acids lack. In this work, we report for the first time a comprehensive molecular-to-process-level study of urea MSA DESs formulated across molar ratios from 1:2 to 1:8, explicitly designed to achieve superacidic environments for Li extraction from clay-hosted ores. Using a combination of Fourier-transform infrared spectroscopy (FTIR), Raman, ultraviolet-visible (UV–Vis), and multinuclear nuclear magnetic resonance (NMR) spectroscopy (^{1}H and ^{13}C), the progressive transformation of the DES structure is elucidated from hydrogen-bond-dominated networks to ionic, protonated media. In addition, Density Functional Theory (DFT) has been employed to calculate interaction energies and global reactivity descriptors, therefore providing theoretical support for the observed behavior of the solvent and electronic delocalization. The extractive performance of these DESs will be tested using Li-bearing clay ore, directly compared with conventional sulfuric, citric, and oxalic acid leaching. Lithium recovery efficiency, selectivity vs. structural elements such as aluminum (Al) and potassium (K), and the role of water addition in controlled acidity and transport properties tuning are emphasized. In linking molecular-scale interactions and computational descriptors to macroscopic leaching outcomes, this work provides a mechanistic framework of superacidic-DES design for complex mineral matrices that can support the transition toward sustainable industrial metal processing. These future efforts will focus specifically on the recovery of extracted elements using electrodialysis and conduct a systematic study of the effects of important parameters on both the leaching and recovery processes.

2. Materials and methods

2.1. Materials

The urea was received from Fluorochem Ltd. (UK). The sulfuric acid (95–98%), citric acid (anhydrous, 99.5–100.5%), 4-nitroaniline (≥99%), and 2,4-dinitroaniline (98%) were received from Sigma-Aldrich, sourced from the USA, Australia, Spain, and China, respectively. The oxalic acid (≥99%) and MSA (≥99%) were purchased from Sigma-Aldrich (Germany). Absolute ethanol (≥99.8%) was supplied by Fisher Chemical (UK), and deuterium oxide (D_2O) was obtained from VWR Chemicals BDH® (Leuven, Belgium). The NMR tubes were purchased from Wilmad-Labglass (Vineland, USA) (500 MHz, OD: 7 mm, length: 7 in., thin wall: 0.43 mm). A coaxial quartz tube was purchased from Norell®, USA (probe: Bruker, tube: 5 mm, OD: 3 mm, length: 50 mm, stem capacity: 175 µL, sample capacity: 285 µL). Quartz cuvettes (wavelength range: 190 nm–2500 nm, path length: 10 mm, volume: 3.5 mL) were received from Best Quality (India). The Li-bearing clay ore used in this study originates from the Valjevo ("Lukavac") sedimentary deposit, located approximately 80 km southwest of Belgrade, Serbia. The PTFE syringe filter (Fisherbrand™, with 0.45 µm pore size and 25 mm diameter) was purchased from Fisher Scientific (UK). The ICP multi-element standard solutions IV certified reference materials were brought from Merck KGaA, Darmstadt, Germany, and used to prepare a standard calibration solution.

2.2. Formulation of urea-MSA DESs

The DES used in this study is urea-MSA in various molar ratios of 1:2 to 1:8. The required amount of urea and MSA was mixed and heated on a hot plate at a temperature of 50 °C to 70 °C until a uniform liquid was obtained. The formed DESs were kept in the tight bottles to prevent any contamination from outside atmospheric conditions. The DESs were used without any further purification. The chemical structures of urea and MSA, along with a photograph of the formulated DESs, are shown in Fig. 1(a)-(c), respectively. As can be seen in Fig. 1(c), DES is not liquid at the ratio of 1:1.

2.1) Determination of Hammett acidity function (H_0)

For measuring the acidity of pure DESs and their aqueous solutions, the Hammett acidity function (H_0) was applied. The H_0 values were determined following the unified Hammett equation [22,23]:

$$H_0 = \rho K_a + \log\left(\frac{[I]}{[IH^+]}\right) \quad (1)$$

where $[I]$ and $[IH^+]$ represent unprotonated and protonated indicator concentrations (or percent), respectively, and the ratio $[I]/[IH^+] = (A/(A_{max}\text{-}A)$ was obtained from absorbance measurements. The method accounts for contributions from both unprotonated and protonated species and thus is applicable over a range of acidity in aqueous and pure DES systems. Aqueous pK_a values of 0.99 for 4-nitroaniline (aqueous DES solutions) and − 4.53 for 2,4-dinitroaniline (pure DESs) were used, where A_{max} is the absorbance of the completely unprotonated indicator, and A is the absorbance in the sample. Details of the acidity measurement of aqueous DES solutions and pure DESs are described in the supplementary data.

2.3. Leaching experiment

The extraction of metals from the Li-bearing clay sample was performed via a batch leaching process designed to maximize the contact between the acidic solvent and the mineral matrix. The initial samples received from the project partner had a particle size of less than 5 mm. These samples were further ground, and the particle size distribution (PSD) of representative subsamples was measured using a Mastersizer under wet dispersion conditions. The resulting d_{80} was 158.41 µm, and this size fraction was subsequently used for the leaching experiments, with no chemical pretreatment applied in order to ensure a direct leaching process. In a typical experiment, the Li-bearing clay sample was mixed with urea-MSA (1:2) or its aqueous solution in a glass vial at a

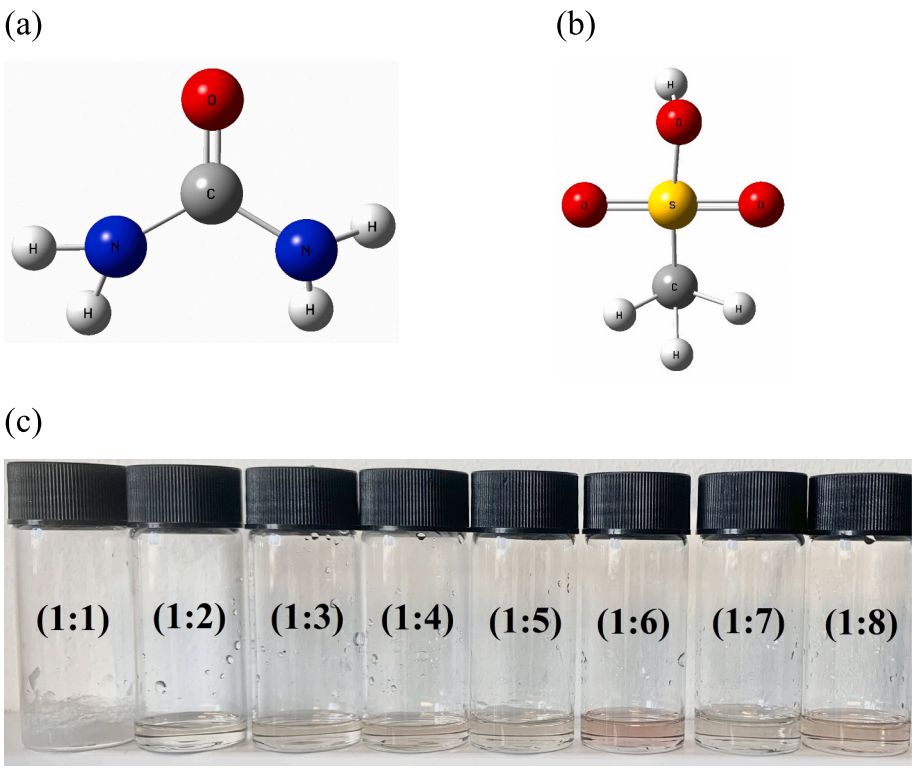

Fig. 1. (a) Chemical structure of urea, (b) chemical structure of MSA, and (c) photo of formulated urea-MSA DESs from a 1:1 ratio to 1:8 ratio.

fixed solid-to-liquid (S/L) ratio of 1:10 (*w/v*). The selection of the 1:2 M ratio, the addition of 20% water, a temperature of 110 °C, and a 150-min duration was based on preliminary screening tests (**Table S1**, Supplementary Material). The mixture was then placed on a magnetic stirring hot plate and heated to 110 °C using a water bath to ensure uniform thermal distribution. The leaching process was maintained for a duration of 2:30 h under constant agitation at 150 rpm. Following the completion of the leaching, the resulting slurry was filtered to isolate the pregnant leach solution (PLS) from the solid mineral residue. For comparative purposes, identical leaching procedures were conducted using 3.33 M oxalic acid, 3.64 M citric acid, and 0.19 M sulfuric acid. To prepare the PLS for elemental quantification, the solution was first passed through 0.45 µm PTFE syringe filters to remove any remaining micro-particulates and was subsequently diluted with deionized water at a specific ratio to bring the metal concentrations within the analytical range of the instrument.

2.4. Characterizations

The FTIR spectrometer (Bruker Alpha spectrometer with Platinum-ATR module) was used to identify the functional groups of DES and hydrogen bond interactions in the wavelength range from 400 to 4000 cm^{-1}. Raman tests were performed using a Bruker SENTERRA II Raman Microscope at room temperature, and the spectra were recorded with an excitation laser wavelength of 532 nm in a range from 100 to 4000 cm^{-1}. The laser power, integration time, co-additions, and objective were respectively fixed at 20 mW, 1000 ms, 30 scans, and 4×. An aluminum metal substrate was employed for sample deposition and measurement to avoid background interference and to provide sample presentation uniformity. Data collection was performed with OPUS software, while analysis and processing were performed with MestReNova software. NMR (^{1}H and ^{13}C) spectra were obtained on a Bruker AM 400 MHz NMR instrument equipped with a 5 mm PABBO BB/19F-1H/D *Z*-GRD probe (Z119470/0185). The experiments were carried out using a normal tube at 298 K and using a coaxial tube at several temperatures: 25 °C, 30 °C, 40 °C, 50 °C, and 60 °C employing the D_2O solvent. The details of sample preparation for NRM are explained in the supplementary data. The spectral width, acquisition time, number of scans, and relaxation delay were adjusted to 10 kHz, 3.28 s, 16, and 1.0 s, respectively, for ^{1}H NMR measurement, while these parameters were adjusted to 29.762 kHz, 1.1 s, 1024, and 2.0 s, respectively, for ^{13}C NMR measurement. All NMR spectra were acquired, processed, and analyzed using TopSpin 4.4.1 software (Bruker Biospin) and MestRenova to ensure accurate spectral acquisition and interpretation over the examined molar ratios. The Brønsted acidity of the pure DESs and their aqueous solutions in terms of H_0 was measured through UV–vis spectroscopy (SPECORD®210 PLUS, Analytik Jena, Germany) using 4-nitroaniline and 2,4-dinitroaniline as basic indicators. The spectra were scanned between 250 nm and 500 nm at room temperature. Bulk chemical compositions were determined by lithium borate fusion followed by inductively coupled plasma–optical emission spectroscopy (ICP–OES) for major elements and inductively coupled plasma–mass spectrometry (ICP–MS) for trace and rare earth elements. Loss on ignition (LOI) was measured gravimetrically. The full analytical dataset, including trace and rare earth element concentrations, is provided in supplementary data, **Table S2**. Mineralogical compositions were determined using X-ray diffraction (XRD) to identify crystalline phases and assess mineralogical changes before and after thermal and leaching treatments. XRD measurements were performed using Cu Kα radiation, scanning from 5° to 70° 2θ with a step size of 0.02°. Phase identification was carried out using standard crystallographic databases (e.g., ICDD PDF-4+). The concentration of Li and other associated elements, including sodium (Na), strontium (Sr), boron (B), manganese (Mn), iron (Fe), magnesium (Mg), calcium (Ca), aluminum (Al), and potassium (K) in PLS was evaluated using an iCAP™ PRO ICP-OES Duo instrument.

2.5. Computational methodology

The DFT is employed to elucidate the molecular interactions and physicochemical properties of urea-MSA DESs, focusing on hydrogen

bonding and potential protonation effects, such as the formation of protonated urea species in high MSA ratios, as observed in experimental vibrational spectroscopy. DFT simulations provide insights into structure-property relationships critical to understanding DES formulation and behavior. All calculations were performed using the GAUSSIAN 16 software package. Molecular geometries of urea, MSA, and their DES complexes were optimized using Becke's three-parameter exchange functional combined with the Lee-Yang-Parr gradient-corrected functional (B3LYP), coupled with the 6–311++G(d,p) basis set and Grimme's D3 dispersion correction with Becke-Johnson damping (empiricaldispersion = gd3bj) to accurately model hydrogen bonding and van der Waals interactions essential for the urea-MSA DES. The 6–311++G(d,p) basis set includes diffuse and polarization functions to describe the electronic structure of hydrogen-bonded and ionic systems effectively. Initially, the geometries of individual urea and MSA molecules were optimized. Subsequently, multiple configurations of the urea-MSA DES at various molar ratios (e.g., 1:2, 1:3, and 1:4, MSA:urea) were optimized, guided by electrostatic potential (ESP) maps to identify key interaction sites. Interaction energies were corrected using the counterpoise method to mitigate basis set superposition errors (BSSE) [24]. The absolute interaction energy ($|\Delta E_{\text{int}}|$) for DES formation was calculated as follows:

$$|\Delta E_{\text{int}}| = E_{\text{formation}} - \sum_{i=1}^{n} E_{\text{fragment }(i)} \tag{2}$$

where $E_{\text{formation}}$ represents the (counterpoise corrected) energies of DES structures. $E_{\text{fragment }(i)}$ is the energy of individual fragment i, calculated within the same formed DES, and n is the number of fragments in the formed DES.

The highest occupied molecular orbital (HOMO) and lowest unoccupied molecular orbital (LUMO) are collectively referred to as the frontier molecular orbitals (FMOs). These orbitals play a critical role in determining the chemical reactivity and stability of molecules. The HOMO represents the ability of a molecule to donate electrons (nucleophilicity), while the LUMO reflects its ability to accept electrons (electrophilicity). The energy difference between these orbitals, known as the energy gap (E_{gap}), is often used as an indicator of molecular stability: smaller gaps generally imply higher chemical reactivity and lower kinetic stability. Based on the FMO energies, a set of global reactivity descriptors was calculated to further characterize the electronic structure and reactivity profile of each system. These include ionization potential (IP), electron affinity (EA), chemical potential (μ), hardness (η), softness (S), electrophilicity index (ω), and electronegativity (χ). The calculations were performed using Koopmans' theorem as a working approximation, wherein the orbital energies are treated as estimates of ionization potential and electron affinity. The descriptors were computed using the following equations:

$$IP = -\mathscr{E}_{\text{HOMO}} \tag{3}$$

$$EA = -\mathscr{E}_{\text{LUMO}} \tag{4}$$

$$\mu \approx -\left(\frac{IP + EA}{2}\right) \approx \frac{\mathscr{E}_{\text{LUMO}} + \mathscr{E}_{\text{HOMO}}}{2} \tag{5}$$

$$\eta \approx \frac{IP - EA}{2} \approx \frac{\mathscr{E}_{\text{LUMO}} - \mathscr{E}_{\text{HOMO}}}{2} \tag{6}$$

$$S \approx \frac{1}{IP - EA} \approx \frac{1}{\mathscr{E}_{\text{LUMO}} - \mathscr{E}_{\text{HOMO}}} \tag{7}$$

$$\omega = \mu^2/2\eta \tag{8}$$

$$\chi = -\mu \tag{9}$$

These values provide a comprehensive framework for interpreting the stability and reactivity trends across urea–MSA complexes with varying stoichiometric ratios. All energy values were expressed in electron volts (eV), with orbital energies extracted from DFT-optimized geometries.

3. Results and discussion

3.1. FTIR and Raman spectroscopy analysis

The structural evolution of the urea-MSA DES system was investigated across molar ratios from 1:2 to 1:8 (urea:MSA) using complementary FTIR and Raman spectroscopy. Fig. 2 shows the FTIR and Raman spectra of DESs and their initial compounds, including urea and MSA. The combined spectroscopic data clearly indicate a composition-dependent transition in the dominant intermolecular forces, shifting from a network defined by strong hydrogen bonding at low MSA concentrations to an environment that progressively exhibits a more pronounced ionic character as the MSA concentration increases. In the high-wavenumber region (3200–3450 cm^{-1}), both techniques tracked the nitrogen–hydrogen (N—H) and hydroxyl (O—H) stretching vibrations, which are the primary indicators of hydrogen bonding. At the low MSA ratios (1:2 to 1:4), significant redshifts were observed in the Raman N—H bands (up to 117 cm^{-1} from the pure urea values), coupled with a shift of the FTIR carbonyl (C=O) stretching peak slightly below the pure urea value of 1674 cm^{-1} [25,26], collectively confirming the formation of a strengthened, cooperative hydrogen-bonded network where urea acts as the HBD and MSA's sulfonic acid (-SO_3H) group acts as the HBA. As the MSA ratio was increased above 1:4, the intensity of the N-H/O-H stretching bands reduced in Raman, and the associated redshifts decreased (Fig. 2(b)). On the other hand, the dominating N—H stretching band in the FTIR spectra, which appeared in the range 3410–3450 cm^{-1}, shifted to a higher wavenumber, contrary to the band intensities in the pure urea, which were 3427.7, 3325.7, and 3254.4 cm^{-1} [25] (Fig. 2(a)). The observations indicate a marked weakening of the urea-related hydrogen bonding, which is consistent with the increased acidity properties and the resultant transition toward proton transfer and the formation of ionic species. This is also evident from the carbonyl stretching band C=O, which appears in the fingerprint region. The Raman C=O band, initially located at 1678.5 cm^{-1} (1:2), progressively shifted to a higher wavenumber (1684.5 cm^{-1}) at the 1:8 ratio, a change mirrored by the shift and intensity reduction of the corresponding FTIR peak. This upward shift indicates that the C=O group becomes less constrained and less involved in the hydrogen-bonding network as the amine (−NH_2) groups become protonated.

More importantly, the C—H stretching region between 2920 and 3060 cm^{-1}, corresponding to the methyl (-CH_3) group of MSA, provided good evidence for the ionic shift. These bands, in both FTIR and Raman spectra, increased in intensity progressively with the increase of the MSA ratio and reached the maximum at 1:8. The observed enhanced intensity reflects the increasing vibrational freedom of the -CH_3 groups as a result of their release from the hydrogen bonding constraints in neutral MSA, which once more strongly supported the dominance of the less-associated MSA anion at higher concentrations. In addition to the above, the change of mode and the eventual disappearance of the peak at 106.5–84 cm^{-1}, above the 1:4 ratio, in the low-frequency Raman region below 400 cm^{-1} indicated a significant structural rearrangement in intermolecular interactions from urea-dominated to MSA-driven. Collectively, the combined FTIR and Raman results substantiate the inference of a dynamic hydrogen bonding network that, upon excess MSA loading, drives the system from a classic DES structure to one possessing characteristics of a protic ionic liquid, a degree of tunability that is highly relevant for tailored applications in green chemistry and materials synthesis. More details of the FTIR and Raman analysis are provided in the supplementary data.

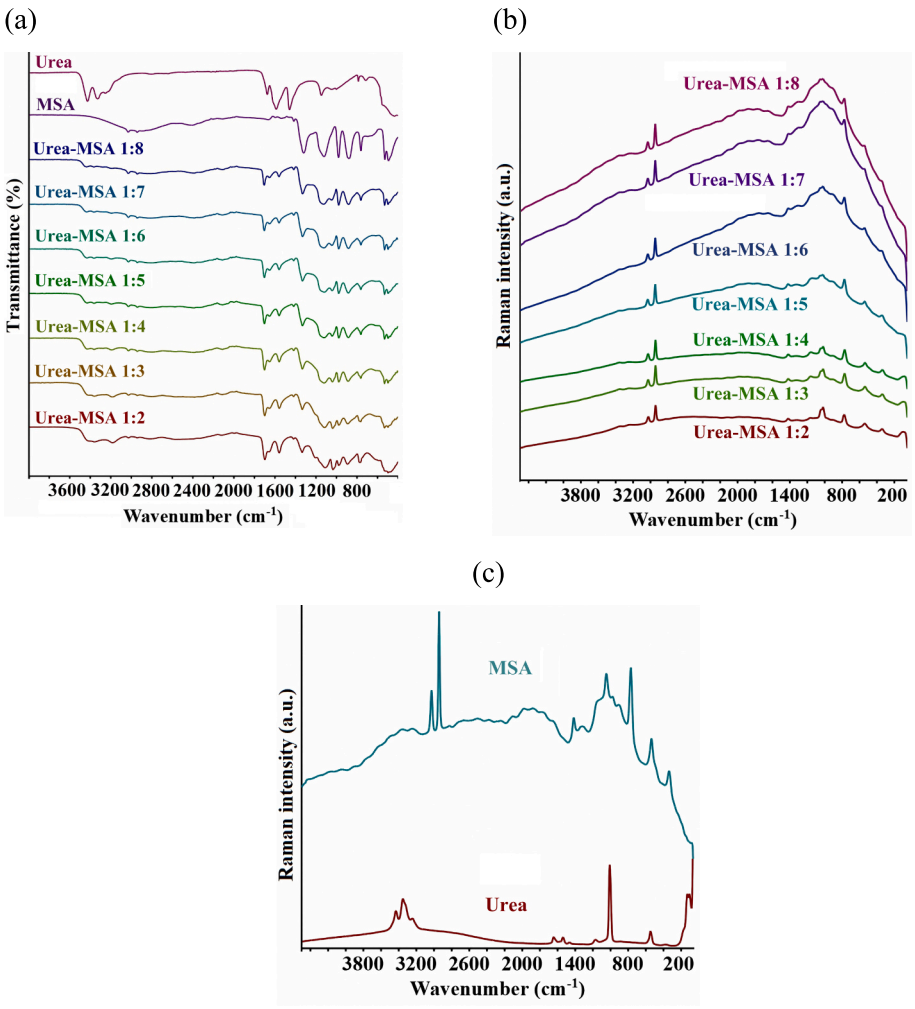

Fig. 2. (a) FTIR spectra of precursors and urea-MSA DESs, (b) Raman spectra of urea-MSA DESs at various molar ratios, and (c) Raman spectra of precursors (urea and MSA).

3.2. NMR spectroscopy analysis

The ^{1}H and ^{13}C NMR spectroscopy provided site-specific insight into the dynamics of hydrogen bonding and changes in the electronic environment within the urea-MSA DES system, covering molar ratios between 1:2 and 1:8 (urea:MSA). The ^{1}H NMR spectra of the initial compounds and DESs are shown in Fig. 3(a) and Fig. 3(b), respectively, and the peak position data are presented in Table 1. Its ^{1}H NMR spectra showed two main signals, the residual water (HDO) signal, which involves labile protons exchanged from the -NH_2 groups of urea and -SO_3H group of MSA, and another non-exchangeable CH_3 proton signal of MSA. The HDO peak, a sensitive probe of the average hydrogen bond strength and acidity, was progressively shifted downfield from 5.04 ppm at the 1:2 ratio to 5.335 ppm at 1:8 (Fig. 3(b)). This continuous downfield movement reflects the substantial rise in overall acidic character and general weakening of the hydrogen bond network, particularly on the interactions involving the -NH_2 protons of urea. This happens with the increase in the molar fraction of highly acidic MSA. Complementing this, the CH_3 proton signal of MSA exhibited a clear upfield shift from 1.659 ppm at 1:2 to 0.883 ppm at 1:8. This progressive increase in shielding (upfield shift) is believed to manifest the transition from specific hydrogen-bonding interactions between the components at low ratios toward a more ionic environment at higher concentrations. In this respect, the MSA anion is less constrained by the network and hence results in reduced deshielding effects on the CH_3 group.

The ^{13}C NMR spectra of the initial compounds and DESs are shown in Fig. 3(c) and Fig. 3(d), respectively, and the peak positions are summarized in Table 1. The ^{13}C NMR data strongly validate these findings by monitoring the electronic environment of the two-key molecular centers: the urea's C═O and the MSA's CH_3. The urea C═O resonance shifted upfield from 160.75 ppm at the 1:2 ratio to 159.87 ppm at 1:8 (Fig. 3(d)). This upfield shift confirms that the urea's -NH_2 groups are active in hydrogen bonding with MSA's sulfonate (-SO_3^-) moiety. Due to hydrogen bonding, electron donation from the -NH_2 groups to the C═O via resonance is reduced, which in turn decreases the deshielding effect on the carbonyl carbon and causes the observed shielding (upfield shift). On the other hand, the carbon signal of MSA-CH_3 initially shifted slightly downfield at 1:2 ratio (37.53 ppm from 36.77 ppm in pure MSA), reflecting the deshielding effect of the new hydrogen bonding environment, but thereafter always shifted progressively upfield to 36.75 ppm at 1:8. This later upfield trend is in agreement with the trend in the ^{1}H data, which indicates that the -CH_3 group becomes progressively shielded as the ionic character dominates and specific hydrogen bonding interactions diminish. Further details regarding the NMR analysis can be found in the Supplementary Data. Taken together, the NMR data provides robust, atomic-level confirmation that the urea-MSA system transitions from a structure dominated by strong, extensive hydrogen bonding at low MSA ratios (1:2 to 1:3) to a dynamic, acidic environment with weakened hydrogen bonds and an accumulation of ionic species at high ratios (1:4 to 1:8). This result is strongly supported by the results of vibrational spectroscopy experiments. The upfield shift of the MSA-CH_3 signals in NMR experiments, which corresponds to

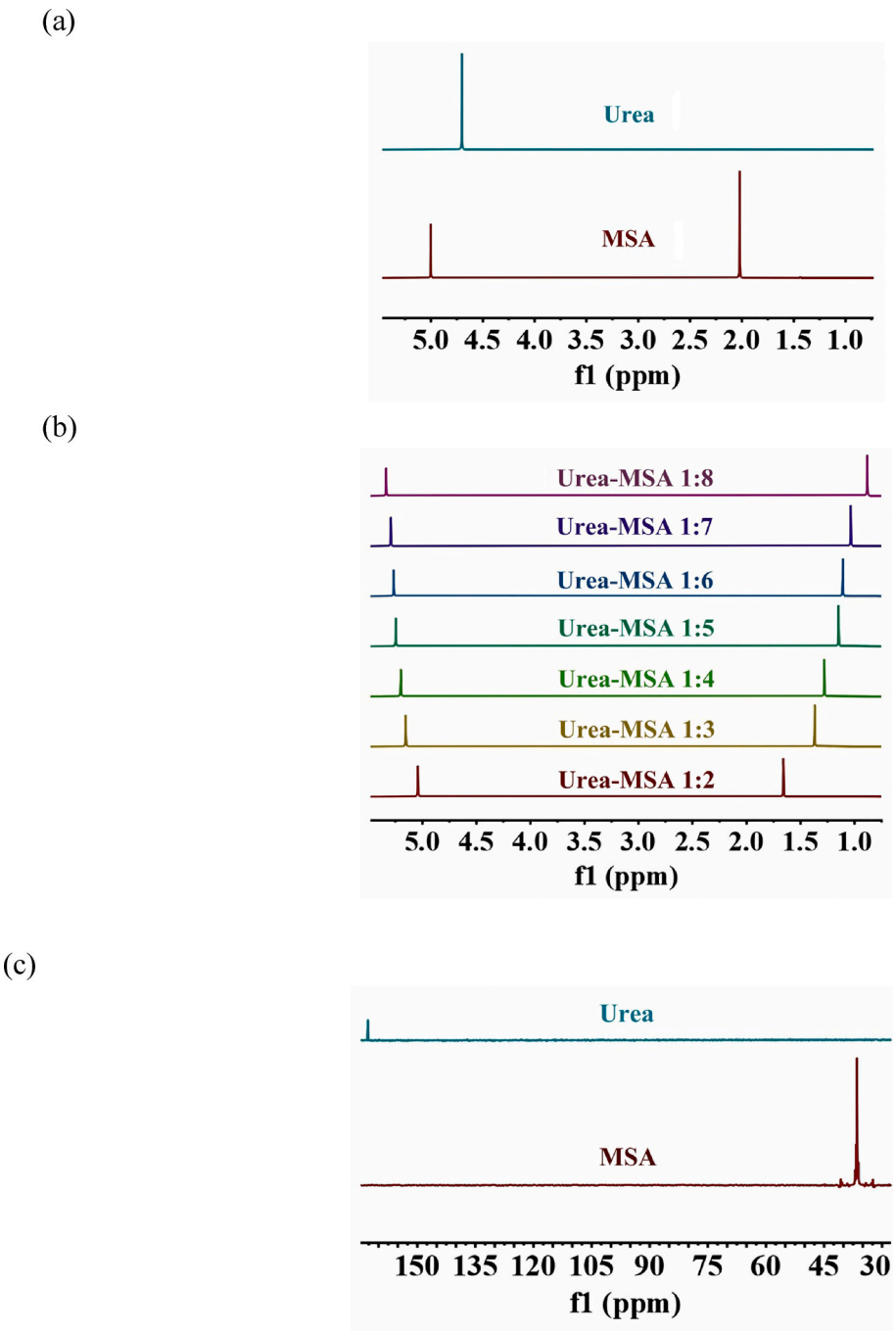

Fig. 3. NMR spectra of urea, MSA, and urea-MSA DESs at different molar ratios, recorded using D_2O as the solvent: (a) ^1H NMR of pure precursors; (b) ^1H NMR of DES complexes; (c) ^{13}C NMR of pure precursors; (d) ^{13}C NMR of DES complexes.

increased shielding and a weakening of hydrogen bonding constraints, is directly consistent with the increased intensity of the C—H stretching bands evident in FTIR and Raman experiments, reflecting increased CH_3 group freedom of the MSA component. Similarly, the downfield shift of the HDO signal in NMR experiments, reflecting a weakening of urea's hydrogen bonding role, is consistent with the decrease in intensity and blue shift of N—H stretching bands evident in FTIR and Raman experiments. Overall, the three types of experiments confirm a consistent multi-scale validation of the structural changes of the system, reflecting a shift from a hydrogen bonding-based DES to a system with increased protic ionic liquid properties.

The results obtained from the analysis of the urea-MSA DESs with the coaxial tube setup, with varying molar ratios of 1:2, 1:5, and 1:8, from 25 °C to 60°C, played a significant role in interpreting the dynamic properties of the system, thereby ensuring that proton exchange is the characteristic that dominates the behavior of the DES. Fig. 4 shows the ^1H and ^{13}C NMR spectra of the urea-MSA DESs with varying molar ratios. The ^1H NMR spectra revealed the dynamic behavior of the system, which clearly showed the existence of fast proton exchange (**Fig. 4**(a), (c), and (e) on the left side). The sharp dominant peaks, corresponding to the averaged signals of the fast-proton-exchanged labile hydrogen atoms (either from MSA-SO_3H/MSA-CH_3 or urea-NH_2), showed a consistent downfield shift with the rise in temperature for all ratios (for instance, from 3.04 ppm at 25 °C to 3.65 ppm at 60 °C for the 1:8 ratio). The

(d)

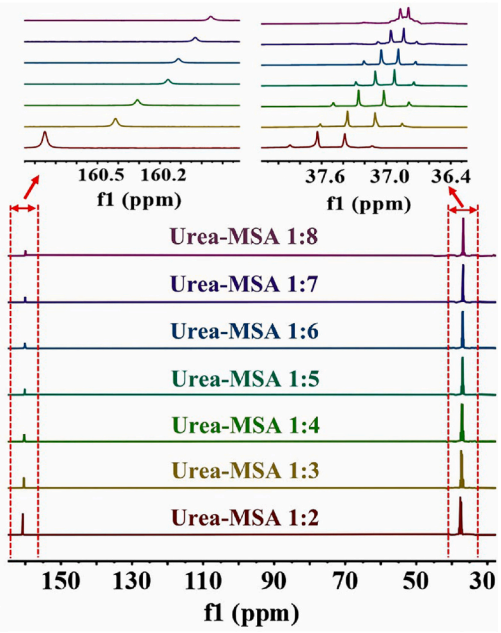

Fig. 3. (*continued*).

Table 1
^{1}H and ^{13}C NMR peak positions and assignments for urea, MSA, and urea-MSA DESs at different molar ratios (recorded in D_2O).

Sample	^{1}H NMR peaks (ppm)	^{1}H NMR assignment	^{13}C NMR peaks (ppm)	^{13}C NMR assignment
Pure urea	4.7	HDO (from -NH_2 exchange)	162.77	C═O
Pure MSA	5.0, 2.02	HDO, -CH_3	36.77	-CH_3
Urea-MSA 1:2	5.04, 1.659	HDO, MSA -CH_3	160.75, 37.53	Urea C═O, MSA -CH_3
Urea-MSA 1:3	5.154, 1.369	HDO, MSA -CH_3	160.41, 37.22	Urea C═O, MSA -CH_3
Urea-MSA 1:4	5.199, 1.281	HDO, MSA -CH_3	160.30, 37.13	Urea C═O, MSA -CH_3
Urea-MSA 1:5	5.246, 1.149	HDO, MSA -CH_3	160.16, 37.0	Urea C═O, MSA -CH_3
Urea-MSA 1:6	5.266, 1.110	HDO, MSA -CH_3	160.11, 36.95	Urea C═O, MSA -CH_3
Urea-MSA 1:7	5.291, 1.036	HDO, MSA -CH_3	160.03, 36.89	Urea C═O, MSA -CH_3
Urea-MSA 1:8	5.335, 0.883	HDO, MSA -CH_3	159.87, 36.75	Urea C═O, MSA -CH_3

downfield shift, which is quantified by a shift of as high as 0.44 ppm for the 1:8 ratio, clearly verifies that with an increase in thermal energy, the dynamical behavior of the hydrogen bonding network increases, thus resulting in a decrease in the shielding effect on the averaged proton environment.

Most importantly, the observation of broad, slow-exchange peaks in the highly downfield region (8.91 ppm–10.33 ppm) at increased temperatures (40 °C–60 °C) signified the onset of a low-intermediate or slow exchange regime. The highly downfield location of these peaks, which shifted from 9.34 ppm at the hydrogen bonding-dominant 1:2 ratio to 10.33 ppm at the ionic 1:8 ratio, is a highly significant observation. The large ratio-dependent shift indicates that the acidity and protonation affinity increase drastically with MSA concentration, thus providing direct proof of the ionic transition facilitated by the increased acidity. The observation of the slow exchange peaks indicates that this phenomenon occurs concurrently with the shift in acidity that depends on the composition. Unlike the highly dynamic proton behavior, the ^{13}C NMR results confirmed the stability of the molecular structure (Fig. 4 (b), (d), and (f) on the right side). The MSA-CH_3 carbon (39.03 ppm–39.65 ppm) experienced a slight downfield shift (0.46 ppm to 0.48 ppm), but the urea C═O carbon had a stable structure with respect to temperature. The result, therefore, confirms that the proton exchange is responsible for the temperature- and composition-dependent behavior of the DES, while carbon atoms are characterized by a stable structural background, unlike the highly dynamic proton. The slight upfield shift that occurred initially in the C═O carbon at the highly acidic ratio of 1:8 confirms the presence of the urea cation species, which has a stable structural integrity. Taken together, the results from the coaxial tube confirm, by providing quantitative characterization of the temperature dependence and identifying the signals of the slowly exchanging protons, the presence of the proton transfer mechanism that supports the changes in hydrogen bonding strength and MSA anion shielding observed in the standard D_2O NMR analysis.

3.3. Hammett acidity function (H_0) analysis

Acidity of pure urea-MSA DESs and their aqueous solutions was determined by the H_0 with 2,4-dinitroaniline and 4-nitroaniline, respectively. The intrinsic acidity of the pure, undiluted urea-MSA DES was measured at all ratios (1:2 to 1:8) using 2,4-dinitroaniline as the indicator, revealing a strong superacidic range. Fig. 5(a) displays the absorbance spectra of 2,4-dinitroaniline in the presence of pure DESs. The H_0 values of pure DES are presented in Table 2. The experimentally determined H_0 values decline progressively and significantly with increasing MSA ratio, commencing in the superacidic region at 1:2 ($H_0 = -4.17$), where 30.35% of the indicator is protonated [IH^+]. Notably, the acidity is moderated to $H_0 = -3.102$ by adding 20% water to the 1:2

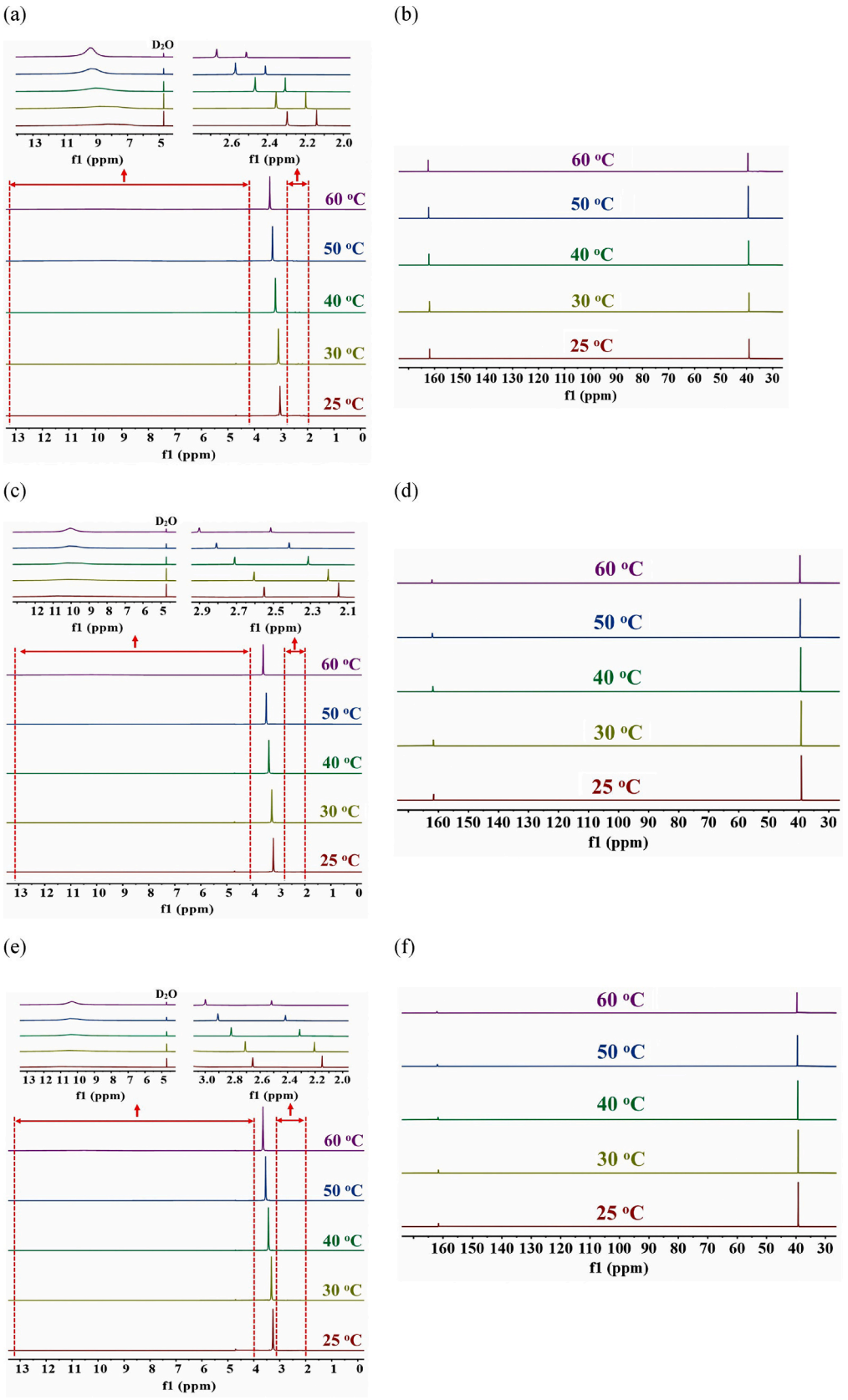

Fig. 4. Temperature-dependent ^{1}H and ^{13}C NMR spectra of urea-MSA DESs, recorded using D_2O as the solvent: ^{1}H NMR of (a) 1:2, (c) 1:5, and (e) 1:8 ratios; ^{13}C NMR of (b) 1:2, (d) 1:5, and (f) 1:8 ratios.

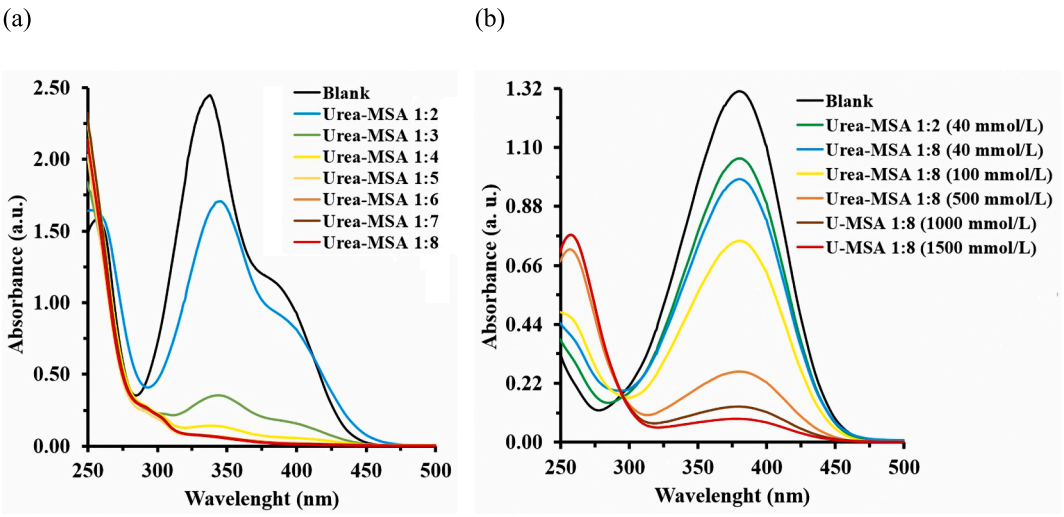

Fig. 5. UV–vis absorbance spectra of indicator probes in urea-MSA DESs: (a) 2,4-dinitroaniline (1.7×10^{-1} mmol/L) in ethanol for 1:2 to 1:8 M ratios; (b) 4-nitroaniline (0.1 mmol/L) in water for 1:2 and 1:8 ratios (40 mmol/L) and 1:8 ratio at varying concentrations (up to 1500 mmol/L).

Table 2
The H_0 values of pure urea-MSA DESs and 80% urea-MSA 1:2 + 20% H_2O at room temperature. (Measured using 2,4-dinitroaniline indicator at 1.7×10^{-1} mmol/L in ethanol).

	A_{max}	[*I*] (%)	[IH^+] (%)	H_0
Blank	2.45	100	0	–
Urea-MSA 1:2	1.70	69.65	30.35	−4.17
80% urea-MSA 1:2 + 20% water	2.360	0.964	0.036	−3.102
Urea-MSA 1:3	0.35	14.49	85.51	−5.30
Urea-MSA 1:4	0.14	5.58	94.42	−5.76
Urea-MSA 1:5	0.073	2.985	97.015	−6.042
Urea-MSA 1:6	0.071	2.891	97.109	−6.056
Urea-MSA 1:7	0.068	2.766	97.234	−6.076
Urea-MSA 1:8	0.067	2.740	97.260	−6.080

ratio (80% urea-MSA 1:2 + 20% water) (Table 2). While this represents a decrease in proton activity compared to the undiluted system, the formulation remains firmly within the superacidic regime. This specific level of "controlled acidity" is critical for the leaching process; it provides sufficient proton activity to disrupt the robust aluminosilicate lattice of the Serbian ore, while the modified transport properties facilitate total lithium mobilization (100% Li extraction) without excessive gangue dissolution. The acidity escalates sharply through the 1:3 ($H_0 = -5.30$) and 1:4 ($H_0 = -5.76$) ratios, where [IH^+] rapidly climbs to 85.51% and 94.42%, respectively. The acidity reaches a maximum plateau of $H_0 = -6.080$ at the 1:8 ratio, with near-complete indicator protonation at 97.26% [IH^+]. This consistent increase in the superacidic nature of MSA-DES formulations unambiguously illustrates the full proton donation capability of MSA unhindered by the presence of water. The pure DES H_0 values are significantly higher than those observed in aqueous solutions and serve to confirm that the undiluted DES structure actively supports a highly superacidic environment provided by MSA. This superacidity occurs due to hydrogen bonding donation from urea's -NH_2 groups to the MSA's –SO_3^-, thereby stabilizing the produced methanesulfonate anion (MSA^-) on proton release, which allows the proton to be donated from MSA to the indicator molecule.

In contrast to the pure system, the H_0 values for the aqueous urea-MSA DESs, measured with 4-nitroaniline, reflect a significant influence from water dilution. Fig. 5(b) displays the absorbance spectra of 4-nitroaniline in the presence of DESs in water at different concentrations. The H_0 values for the aqueous urea-MSA DESs are presented in Table 3. At a low concentration of 40 mmol/L, increasing the MSA ratio from 1:2 to 1:8 results in only a moderate decrease in H_0, from 1.62 to 1.47. The observed fairly weak to strong acidity in diluted samples is due to the proton acceptor nature of water, which reduces the intrinsic acidity of

Table 3
The H_0 values for aqueous urea-MSA (1:8) at various concentrations (40–1500 mmol/L) compared with literature data. (Measured using 4-nitroaniline indicator at 0.1 mmol/L at room temperature).

Sample	A_{max}	[*I*] (%)	[IH^+] (%)	H_0
Blank	1.31	100	0	–
Urea-MSA 1:2 (40 mmol/L)	1.06	80.87	19.13	1.62
Urea-MSA 1:8 (40 mmol/L)	0.98	75.07	24.93	1.47
Urea-MSA 1:8 (100 mmol/L)	0.75	57.36	42.64	1.12
Urea-MSA 1:8 (500 mmol/L)	0.26	20.14	79.86	0.39
Urea-MSA 1:8 (1000 mmol/L)	0.13	10.11	89.89	0.04
Urea-MSA 1:8 (1500 mmol/L)	0.09	6.70	93.30	−0.15
[Mimps][H_2SO_4] [27] [a]	0.172	55	45	1.07
[Mimps][HCl] [27] [a]	0.186	59	41	1.15
[Mimps][Tfs] [27] [a]	0.208	66	34	1.28
[Bimps][H_2SO_4] [27] [a]	0.186	59	41	1.14
[Bimps][HCl] [27] [a]	0.197	63	37	1.22
[Oimps][H_2SO_4] [27] [a]	0.197	62	38	1.21
[Oimps][HCl] [27] [a]	0.223	71	29	1.38
[choline][HSO_4] [28] [b]	1.19	81.5	18.5	1.63
[choline][H_2PO_4] [28] [b]	1.27	86.9	13.1	1.81
[DMEA][HSO_4] [28] [b]	0.43	29.5	70.5	0.61
[DMEA][H_2PO_4] [28] [b]	1.20	82.2	17.8	1.65
[PSMim][HSO_4] [29] [c]	1.393	59.2	40.8	1.15
[PSMim][H_2PO_4] [29] [c]	1.912	81.3	18.7	1.63
[PSPy][HSO_4] [29] [c]	1.537	65.3	34.7	1.26
[PSPy][H_2PO_4] [29] [c]	2.038	86.6	13.4	1.80
[PSTma][HSO_4] [29] [c]	1.689	71.8	28.2	1.40
[PSPy][HSO_4] [29] [c]	1.537	65.3	34.7	1.26
[C_3SO_3Hmim][HSO_4] [30] [a]	0.64	67	33	1.30
[C_3SO_3Hmim][cl] [30] [a]	0.80	84	16	1.71
[DMEA][cl] [31] [b]	2.467	80.7	19.3	1.61
[DMEA][OAc] [31] [b]	1.972	64.5	35.5	1.25
[DMEA][HSO_4] [31] [b]	0.816	26.7	73.3	0.55
ChCl-AP (1:2) [32] [d]	0.998	94.6	5.4	2.23
ChCl-MCA (1:2) [32] [d]	0.790	74.9	25.1	1.46
ChCl-TCA (1:2) [32] [d]	0.508	48.2	51.8	0.96

[a] The concentrations of IL and 4-nitroaniline were 50.0 mmol/L and 3 mg/L in water, respectively.
[b] The concentrations of IL and 4-nitroaniline were 20.0 mmol/L and 100 mg/L in water, respectively.
[c] The concentrations of IL and 4-nitroaniline were 5.0 mmol/L and 10 mg/L in dichloromethane, respectively.
[d] The concentrations of DES and 4-nitroaniline were 40.0 mmol/L and 10 mg/L in water, respectively.

MSA via the creation of hydrated protons, thus rendering the H_0 value higher compared to the pure DES. This distinction is fundamental: whereas the pure and 80% DES systems operate in a superacidic regime capable of mineral lattice disruption, the aqueous systems are "leveled" by water, resulting in a loss of the unique solvent structure required for efficient clay-hosted lithium extraction. However, the effect of concentration is intense: when the 1:8 DES concentration of 40 mmol/L was increased to 1500 mmol/L, H_0 drastically decreased from 1.47 to −0.15 while the [IH^+] fraction increased dramatically from 24.93% to 93.30%. The deeply negative H_0 value of −0.15 for 1500 mmol/L indicates that at this high concentration, the dilution effect of water is further overridden, which enhances the proton donation capability of MSA.

Comparison with other DESs and ionic liquids (ILs) screened under similar conditions (Table 3) revealed that the urea-MSA has a moderate to strong acidity profile depending on concentration. For example, ChCl-based DESs with weaker acids, such as ChCl-acetophenone (ChCl-AP, 1:2, $H_0 = 2.23$) and ChCl-monochloroacetic acid (ChCl-MCA, 1:2, $H_0 = 1.46$), show higher H_0 values, reflecting their lesser acidity because of

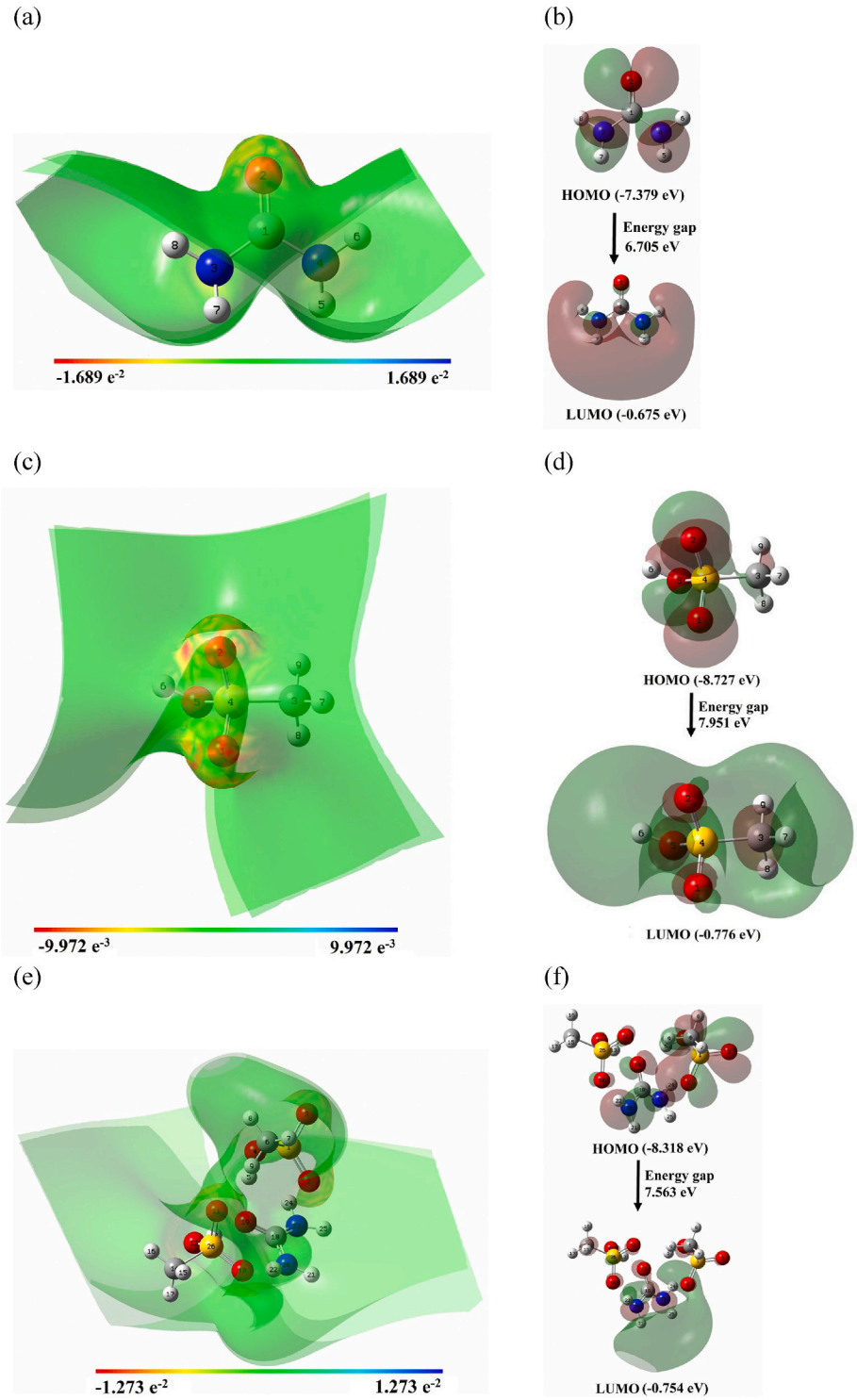

Fig. 6. Optimized geometries and electronic properties of precursors and complexes: (Left) ESP maps and (Right) HOMO–LUMO distributions for (a–b) urea, (c–d) MSA, (e–f) urea-MSA 1:2, (g–h) urea-MSA 1:3, and (i–j) urea-MSA 1:4.

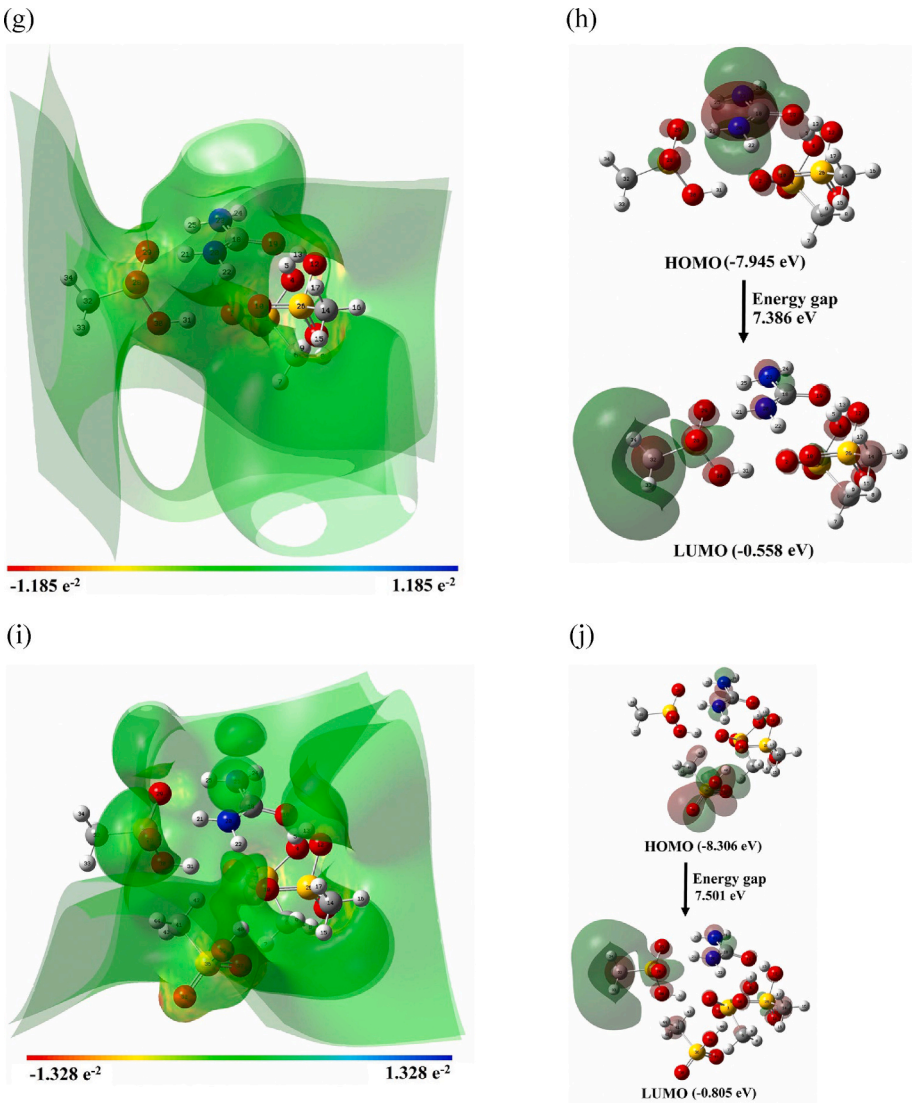

Fig. 6. (*continued*).

the weaker proton-donating ability of acetophenone ($pK_a \approx 20$) and monochloroacetic acid ($pK_a \approx 2.86$) than that of MSA. ChCl-trichloroacetic acid (ChCl-TCA, 1:2, $H_0 = 0.96$) with a higher acidic pK_a (≈ 0.66) also has a lower H_0 than that of urea-MSA 1:2 ($H_0 = 1.62$), suggesting that MSA acidity is moderated by the steric factors of urea and dilution with water. However, at 1500 mmol/L (1:8), H_0 of urea-MSA $= -0.15$ is higher than for ChCl-TCA and the majority of ILs, suggesting higher acidity at high concentrations. Conversely, ILs that are weaker acids, such as [Choline][H_2PO_4] ($H_0 = 1.81$) and [C_3SO_3Hmim][Cl] ($H_0 = 1.71$), possess larger H_0 values, reflecting less proton donation by $H_2PO_4^-$ ($pK_a \approx 7.2$) and Cl^-. ILs with sulfuric acid derivatives, such as [Mimps][H_2SO_4] ($H_0 = 1.07$) and [Bimps][H_2SO_4] ($H_0 = 1.14$), are akin to urea-MSA 1:8 at 40 mmol/L ($H_0 = 1.47$) but are dependent upon the imidazolium cation structure and solvent system (e.g., 50.0 mmol/L in water). This analysis confirms that the intrinsic acidity of the urea-MSA system is highly tuneable and that the absence of water allows MSA to fully facilitate the structural transition into a strong superacidic, protic ionic regime.

3.4. Computational results and analysis

To investigate the electronic behavior, stability, and reactivity of the urea-MSA DES system, DFT calculations were performed to compute global reactivity descriptors for isolated urea and MSA, as well as their complexes at molar ratios of 1:2, 1:3, and 1:4 (MSA:urea). Multiple geometries of the urea-MSA DESs at 1:2, 1:3, and 1:4 M ratios were optimized, with the most stable geometry (highest $|\Delta E_{int}|$) selected for analysis; other geometries are provided in **Fig. S1** of the supplementary data. ESP maps (Fig. 6, left side) and HOMO/LUMO distributions (Fig. 6, right side) show the urea, MSA, and their DES complexes' electronic structure and reactivity. In urea, negative electron density is localized on the C═O group, which is thereby a primary location for the acceptance of hydrogen bonds, and positive density is on the NH_2 groups, making them to function as HBDs (Fig. 6(a)). MSA shows positive density in the vicinity of the CH_3 and OH groups and negative density on the oxygen atoms of the SO_3H group, which are HBAs (Fig. 6(c)). In the 1:2 urea-MSA complex, the negative density is primarily on the SO_3H oxygen atoms of MSA and partially on urea's C═O, whereas the positive density is delocalized on MSA's CH_3 and urea's NH_2 groups (Fig. 6(e)). The same trends are observed in the 1:3 and 1:4 complexes (Fig. 6(g)-(i)), in which the 1:4 complex contains more negative density on SO_3H oxygen atoms that are farther from urea. This suggests that the hydrogen bond interaction between NH_2 groups of urea (donors) and SO_3H oxygen atoms of MSA (acceptors) is disrupted, as the electron density is less available to bond with the hydrogen atoms of urea. The increasing intergroup distance and reduced interaction point toward hydrogen bond weakening

from steric crowding or competitive interactions (i.e., protonation of urea or ionic interactions) as the system is dominated by MSA molecules. NMR, FTIR, and Raman results confirm this, witnessing weaker hydrogen bonding at high ratios of MSA.

As summarized in Table 4, for isolated urea, the $\mathcal{E}_{HOMO}$ was −7.379 eV, $\mathcal{E}_{LUMO}$ was −0.675 eV, yielding a HOMO-LUMO gap of 6.705 eV and an ω of 2.419 eV, indicating moderate electron-donating ability. MSA showed stronger electron-withdrawing behavior, with a $\mathcal{E}_{HOMO}$ of −8.727 eV, $\mathcal{E}_{LUMO}$ of −0.776 eV, a larger gap of 7.951 eV, and ω of 2.839 eV. The μ values for MSA and urea are −4.751 eV and − 4.027 eV, respectively, suggesting a higher reactivity of MSA than urea. The $|\Delta E_{int}|$ data in Table 4 shows a consistent increase with rising MSA ratio, moving from 1.583 eV (1:2) to 2.590 eV (1:3) to 3.237 eV (1:4). This trend evidences an increasingly strong stabilizing intermolecular force at higher ratios. Importantly, since the ESP maps and experimental data confirm that traditional hydrogen bonds are weakening, it is due to the increased contribution of secondary electrostatic interactions - mainly the protonation of urea's C═O or NH_2 groups by MSA's acidic protons, or even the formation of highly charged SO_3^- ionic species. The E_{gap} ranges from 7.563 eV for 1:2 to 7.386 and 7.501 eV for 1:3 and 1:4, respectively, reflecting the consistency of electronic stability with stoichiometric ratios. From these, it is evident that the E_{gap} values for the studied complexes are relatively constant, indicating that the global electronic stability of the complexes remains unchanged with changes in stoichiometry. The IP and EA define the system's ability to donate and accept electrons, respectively. Complex 1:3 showed the lowest IP, 7.945 eV, as well as the lowest EA, 0.558 eV. Consequently, this ratio is the most susceptible to oxidation (facilitating electron donation), but it presents the least propensity to accept electrons. These values are used to calculate the remaining global reactivity descriptors. The μ reflects the tendency of electrons to escape the system. It reduces less negatively from −4.536 eV (1:2) to −4.252 eV (1:3). The present fluctuation is consistent with the experimental evidence of a disrupted hydrogen bond network, owing to the attenuation of the electron-donating capability of the urea component. The μ then becomes more negative at 1:4–4.556 eV, reflecting the dominance of high MSA content. The χ follows the inverse trend with μ, having the lowest χ for the 1:3 complex at 4.252 eV. The η measures the resistance to charge transfer. The S, the inverse of η, indicates reactivity. The 1:3 complex has the lowest η (3.693 eV) and the highest S (0.135 eV^{-1}). The 1:3 ratio may represent a crucial structural crossover point when the ideal hydrogen bonding balance is obtained just before the system quickly switches toward ionic stabilization, as this increased softness suggests a peak in chemical reactivity.

These findings emphasize the tuneable physicochemical properties of urea-MSA DESs, where the variation in molar ratios will balance stability with reactivity and have great potential in applications such as metal extraction. For applications requiring strong coordination, the lower ratios (e.g., 1:2) are electronically favorable due to their strong hydrogen bonding network and the highest localized electron-donating capability of the urea component. Although the 1:4 ratio exhibited a slightly more negative chemical potential (μ), this value reflects the enhanced thermodynamic stability of the entirely rearranged ionic system ($UreaH^+/MSA^-$ clustering). In contrast, the μ value of 1:2 (−4.536 eV) represents the optimal donor capacity of the urea NH groups needed for charge-transfer coordination with the metal ions. Contrarily, the DES systems that presented higher MSA ratios, like 1:4, were dominated by the methanesulfonate anion and the protonated urea cation species. That resulted in far weaker hydrogen bonding. Based on the electronic and structural analyses, the ratio 1:2 is theoretically preferred for metal extraction applications under strong coordination mechanisms. That would provide the most favorable specific electronic environment and structural stability for metal complexation. Based on these theoretical comparisons, the 1:2 ratio was selected for the metal extraction experiments. These computational findings provide a theoretical roadmap for the macroscopic behavior of the urea-MSA system. The consistent increase in $|\Delta E_{int}|$ from 1.583 eV to 3.237 eV as the MSA ratio rises indicates a fundamental shift from a hydrogen-bond-dominant structure toward a more cohesive, ionic-like environment ($ureaH^+/MSA^-$ clusters). This evolution is significant for its impact on acidity; as the interaction energy increases, the MSA protons become more delocalized—a trend reflected in the peak chemical softness (S = 0.135 eV^{-1}) at the 1:3 ratio. While the 1:3 and 1:4 ratios suggest high theoretical reactivity, the 1:2 ratio was identified as the preferred candidate for metal extraction. Its chemical potential (μ = −4.536 eV) reflects an optimal balance: it is sufficiently acidic to disrupt mineral lattices while retaining the necessary electron-donating capacity for charge-transfer coordination with liberated metal ions. Thus, these global reactivity descriptors justify the selection of the 1:2 M ratio as the primary lixiviant for the experimental validation that follows in this study.

3.5. Analysis of extraction efficiency

The Li-bearing clay sample was extracted using the urea-MSA 1:2 system, and its evaluation depicted a potent and selectively efficient leaching profile, establishing its utility as a high-performance solvent for resource recovery. Experimental data presented in Fig. 7 show that the system attains different peak extraction efficiencies depending on the concentration of the solvent, where the formulation of 80% urea-MSA 1:2 + 20% water yields an exceptional value of extraction, 100% for Li, Na, and Sr, and 98% for B. In fact, the supremacy of the 1:2 ratio is deeply rooted in the synergy that exists among its functional groups in the leaching process. The $–SO_3^-$ in MSA serves as the primary proton source by establishing a superacidic environment for the disruption of oxygen-sharing bonds in the silicate layers of the clay. In the meantime, the $–NH_2$ and C═O groups of urea act as powerful coordination sites. Spectroscopy indeed confirms that at the ratio of 1:2, these functional groups of urea are not yet fully sequestered through protonation and thereby act as active ligands-solvating and stabilizing the released metal cations and hindering reprecipitation, which preserves high kinetic drive. This mechanism is evidenced by the high extraction of Li and Sr compared to traditional mineral acids. Comparison of the studied 80% urea-MSA (1:2) + 20% water with the traditional mineral and organic acids reveals the tremendous superiority of the new system in the leaching process. Although 3.33 M oxalic acid is also efficient for the extraction of 100% Li, its efficiency with other essential elements is found to be substantially lower, and only 10% for Mn and 41% for Fe. However, the 80% urea-MSA system proved more efficacious with these essential elements, with the extraction of higher amounts of Mn (87%) and Fe (59%). Moreover, 0.19 M sulfuric acid, the common industrial mineral acid, was found to be the least effective on the sedimentary sample, with the extraction of only 4% Li, 1% Mn, and 1% Fe.

Table 4
Electronic parameters of isolated urea, MSA, and their corresponding DES complexes. (All values are reported in eV unless otherwise specified).

System	$\lvert\Delta E_{int}\rvert$ (eV)	E_{HOMO} (eV)	E_{LUMO} (eV)	E_{gap} (eV)	*EA = -E LUMO*	*IP = -E HOMO*	μ (eV)	η (eV)	S (eV^{-1})	ω (eV)	χ (eV)
Pure urea	–	−7.379	−0.675	6.705	0.675	7.379	−4.027	3.352	0.149	2.419	4.027
Pure MSA	–	−8.727	−0.776	7.951	0.776	8.727	−4.751	3.975	0.126	2.839	4.751
Urea-MSA 1:2	1.583	−8.318	−0.754	7.563	0.754	8.318	−4.536	3.782	0.132	2.720	4.536
Urea-MSA 1:3	2.590	−7.945	−0.558	7.386	0.558	7.945	−4.252	3.693	0.135	2.447	4.252
Urea-MSA 1:4	3.237	−8.306	−0.805	7.501	0.805	8.306	−4.556	3.751	0.133	2.767	4.556

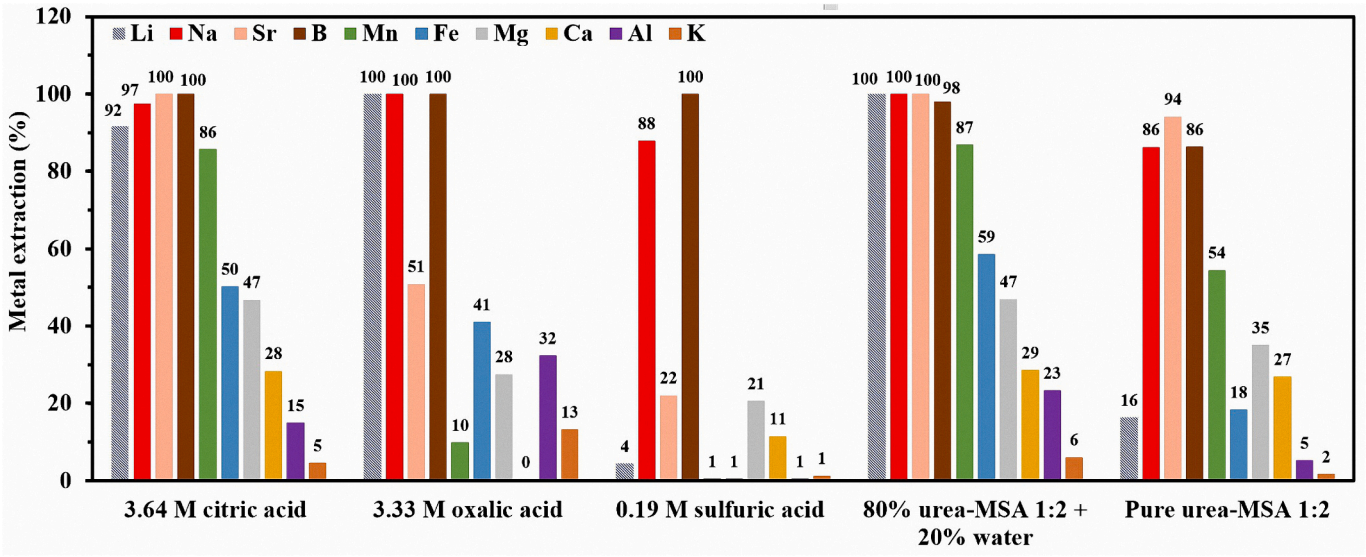

Fig. 7. Comparative efficiency of metal extraction from Li-bearing clay ore using urea-MSA 1:2 formulations and conventional acidic leaching agents.

Additionally, the 3.64 M citric acid was also inefficient on the sample, with the extraction of only 92% Li and 50% Fe.

Although the pure urea-MSA DES has a higher intrinsic acidity with an H_0 value of −4.17, the role of hydration proved key for practical application.The pure formulation demonstrated notably reduced ion extraction efficiency with a Li value of 16%, coupled with reduced yields for Na (86%), Sr (94%), and B (86%). This poor performance in the anhydrous state is attributed to the high viscosity and restricted ion mobility inherent in the dense, hydrogen-bonded ionic network of the neat DES. By contrast, the 80% urea-MSA 1:2 + 20% water mixture retains a superacidity character (H_0 = -3.102) which offers adequate "proton pressure," while the added water dramatically enhances mass transfer. The spectroscopic observations detailed in Sections 3.1 and 3.2—specifically the shift toward ionic character and the protonation of urea—are key to understanding this. In the pure DES, tight ion-pairing limits the availability of active species. The addition of 20% water facilitates the dissociation of these tight clusters, reducing the viscosity and effectively "unlocking" the superacidic protons. This allows for rapid diffusion into the recalcitrant aluminosilicate lattice of the clay, while simultaneously facilitating the outward transport of solvated metal ions. Furthermore, the 20% hydration level is essential for maintaining the "coordination window." As corroborated by DFT calculations (showing an electronically favorable chemical potential of −4.536 eV), the water molecules assist in balancing high proton activity with the ligand-like coordination capacity of the urea components. In the pure DES, the active functional groups of urea are too heavily sequestered by protonation or tight ionic clustering to effectively coordinate liberated cations. With 20% water, the system transitions to a more reactive ionic medium where urea and methanesulfonate species are sufficiently "free" to stabilise Li^+ and other target metals in solution. This stabilization prevents the reprecipitation of metal salts on the mineral surface, which would otherwise create a kinetic "bottleneck."

A critical observation in the extraction profile is the relative selectivity of the 80% urea-MSA 1:2 + 20% water system against common structural components. While extraction for energy-critical metals was near total, Al extraction was limited to 23%, Ca to 29%, and K was restricted to only 6%. This notable discrepancy between high-yield extraction of target metals and the lower mobilization of structural impurities represents a significant industrial advantage. For example, while 3.33 M oxalic acid achieved 100% Li extraction, it extracted significantly higher amounts of structural impurities, including 32% Al and 13% K, while failing to mobilize Ca (0%). 3.64 M citric acid similarly mobilized 15% Al, 28% Ca, and 5% K despite lower Li extraction. Even 0.19 M sulfuric acid, despite its poor efficiency, extracted 1% Al, 11% Ca, and 1% K. Ultimately, the merging point of 100% key component recoveries in the 80% urea-MSA 1:2 + 20% water mixture validates that such a molar ratio is indeed the best form of structural integrity for maximum metal extraction. With the ability to remain superacidic and the retention of its ligand functionality for metal coordination, this DES mixture presents itself as a very valuable and viable agent for advanced metal extraction in lithium clays.

In order to assess the efficiency of the proposed system, a comparative study was conducted with the 80% Urea-MSA (1:2) + 20% H_2O mixture with other conventional lixiviants, including sulfuric acid, citric acid, and oxalic acid. The comparison is provided in Table 5, which shows the distinct leaching behavior according to the chemical properties of the lixiviant and the mobility of the protons. Sulfuric acid has shown high inherent selectivity, but the efficiency of lithium extraction was very low (4%), which indicates that the dissociating nature of the mineral acid alone is not enough to leach out the lithium ions from the clay matrix. Among the organic lixiviants, oxalic acid has shown 100% efficiency in the extraction of lithium, but the selectivity was very poor, which resulted in excessive dissolution of the aluminosilicate matrix (32% Al and 13% K). Such non-selective behavior makes downstream purification more difficult and uses more reagents. In contrast, the pure urea-MSA 1:2 DES showed high selectivity, but the efficiency of the Li extraction was found to be low (16%). Although the optimized system showed high selectivity, the addition of 20% water resulted in a 'surgical' extraction profile, where the efficiency of the Li extraction was found to be 100%, and the dissolution of impurities was found to be low (23% Al and 6% K) compared to the oxalic acid system. This results in a high Li/Al selectivity ratio of 4.35 and a Li/K ratio of 16.67. This performance is due to the superacidic nature of the DES, with $H_0 = -3.102$, which provides the chemical potential to release the intercalated

Table 5
Comparative analysis of leaching performance and selectivity.

Leaching agent	Li Ext. (%)	Al Ext. (%)	K Ext. (%)	Li/Al selectivity	Li/K selectivity
Urea-MSA 1:2 + 20% H_2O	100	23	6	4.35	16.67
3.33 M oxalic acid	100	32	13	3.13	7.69
3.64 M citric acid	92	15	5	6.13	18.40
0.19 M sulfuric acid	4	0.5	1.32	8.00	3.03

lithium. At the same time, the dense hydrogen-bonded network is coordinated with the structural metal ions, while the water content enables the mobility of protons, thereby preventing the complete degradation of the clay lattice. This demonstrates the high potential of hydrated urea-MSA DESs as sustainable systems with minimal downstream processing required to separate the extracted metals.

The ability to recycle and reuse these solvents is one of the main characteristics of DESs. This is the key concept of sustainable metal recovery. Following the liberation of metal ions, the urea–MSA system can technically be regenerated. This involves removing the captured metals using downstream methods, such as electrodialysis, and then readjusting the water content and chemical mixture to its original state. Although the reuse of solvents was not included in the scope of this first research on the mechanisms of dissolution, the ongoing work carried out in the Li4Life project has been focused on the rigorous evaluation of the stability and retention of the performance of these solvents after multiple leaching cycles. This includes identifying potential degradation pathways and optimizing regeneration protocols to ensure long-term process viability. Finally, assessment of the economic viability of the proposed novel leaching system is a critical step toward moving from basic science to industrial application. A comprehensive Techno-Economic Analysis (TEA) is required to accurately estimate the total operating costs, considering intricate factors such as solvent recovery efficiency, energy efficiency, and waste management costs. Although the detailed TEA is currently underway as part of the Li4Life project [33,34] (a Horizon Europe research project on sustainable Li extraction and processing, with UK participation supported by UK Research and Innovation, UKRI), several economic factors can be qualitatively identified from the present study. For example, the exceptionally high selectivity of the 80% urea–MSA 1:2 + 20% water system, enabling 100% extraction of Li with co-leaching only 6% K, provides a 'selectivity credit' that reduces the complexity and cost of downstream processing. Another economic benefit is the opportunity to potentially switch from a 'use-and-discard' to a 'recovery-and-reuse' approach via electrodialysis, which is not commonly achievable with conventional inorganic acids.

4. Conclusion

This study reports the first comprehensive molecular-to-process-level characterization of urea–methanesulfonic acid (MSA) DESs across molar ratios from 1:2 to 1:8, demonstrating potential as sustainable, high-performance solvents for metal extraction. Through an experimental, theoretical framework integrating FTIR, Raman, NMR, UV–Vis spectroscopy, and DFT calculations, structural evolution and acidity modulation governing DES functionality were elucidated. Spectroscopic data revealed a dynamic shift toward an increasingly ionic environment at higher MSA ratios; DFT interaction energies, global reactivity descriptors confirmed that intermediate compositions balance electronic delocalization with coordination capability. Specifically, the urea–MSA (1:2) system emerges as an optimal coordination window where urea retains ligand-like character while maintaining sufficient superacidic proton activity ($H_0 = -3.102$) to disrupt mineral lattices. The practical efficacy of this design is proven by the leaching of lithium-bearing clay, where an 80% urea–MSA (1:2) formulation achieved 100% extraction of Li, Na, and Sr, significantly outperforming conventional sulfuric acid and citric acid. A critical industrial advantage of this system is its superior selectivity; the DES leached significantly less structural Al and K than oxalic acid, which simplifies downstream purification and reduces processing complexity. Furthermore, the system offers clear green advantages for industrial applications, as the components are biodegradable and possess low volatility compared to traditional hazardous mineral acids. By operating at moderate temperatures with high selectivity, this recyclable DES provides a scalable, energy-efficient, and environmentally responsible pathway for the global lithium supply chain.

Furthermore, while this work demonstrates the high performance of the urea–methanesulfonic acid system in the primary extraction phase, the subsequent recovery of metals from the PLS is essential for a complete resource recovery cycle. This is what the ongoing investigations for the Li4Life project aim to do. This includes the evaluation of electrodialysis, solvent extraction, and ion exchange methods. The discoveries made through these investigations will be discussed in a future publication to give an overview of the viability of the entire process for the synthesis of materials and green chemistry.

Future work will explore, within the Li4Life project, the application of these DESs to a broader range of primary ores and secondary sources. Building on the fundamental mechanisms and selectivity identified in this study, subsequent efforts will focus on the integrated recovery of extracted elements using electrodialysis and the systematic optimization of solvent regeneration protocols. Furthermore, the development of a comprehensive techno-economic and life-cycle assessment will be undertaken to quantify the industrial viability and environmental benefits of this circular extraction model. Overall, this work provides a sound basis for the rational design of superacidic DES-based solvent systems that meet the rigorous demands of sustainable and circular critical-metal recovery.

CRediT authorship contribution statement

Hosein Ghaedi: Conceptualization, Data curation, Formal analysis, Investigation, Methodology, Software, Validation, Writing – original draft. **Cristian Serrano Araya:** Formal analysis, Investigation, Methodology, Validation, Writing – review & editing. **Payam Kalhor:** Formal analysis, Software, Validation, Writing – review & editing. **Cora Dawson-Jones:** Writing – review & editing. **Enrico Ferrari:** Writing – review & editing. **Tasnim Munshi:** Formal analysis, Writing – review & editing. **Ian Scowen:** Writing – review & editing, Formal analysis. **Yousef Ghorbani:** Conceptualization, Data curation, Formal analysis, Funding acquisition, Software, Supervision, Validation, Writing – review & editing.

Declaration of competing interest

The authors declare that they have no known competing financial interests or personal relationships that could have influenced the work reported in this paper.

Acknowledgements

This publication is part of the Li4Life project. UK participants in Horizon Europe Project Li4life - Novel Domestic Battery Grade Lithium Carbonate Value Chain for Green Life are supported by UK Research and Innovation (UKRI) grant number 10103347 (University of Lincoln). This project has also received funding from the European Union's Horizon Europe research and innovation programme under grant agreement N° 101137932, and all results can be found on its official website [33] and social channels [34]. The author gratefully acknowledges the Bridge Centre and the Joseph Banks Laboratories at the University of Lincoln for providing access to FTIR, Raman spectroscopy, NMR, and UV–Vis spectroscopy facilities.

Appendix A. Supplementary data

Supplementary data to this article can be found online at https://doi.org/10.1016/j.seppur.2026.137148.

Data availability

Data will be made available on request.

References

[1] J.C. Barbosa, R.S. Pinto, J.P. Serra, C.M. Costa, S. Lanceros-Mendez, R. Gonçalves, Lithium based battery systems: technological and environmental challenges and opportunities, J. Mater. Chem. A 13 (42) (2025) 35952–35975.

[2] P. Parvizi, M. Jalilian, A.M. Amidi, M.R. Zangeneh, J.-R. Riba, From present innovations to future potential: the promising journey of Lithium-ion batteries, Micromachines (2025) 194.

[3] T.R. Benson, M.A. Coble, J.H. Dilles, Hydrothermal enrichment of lithium in intracaldera illite-bearing claystones, Sci. Adv. 9 (35) (2023) eadh8183.

[4] L. Zhang, S. Shao, B. Li, H. Wang, H. Zhang, Y. Wei, A green and efficient process for extracting lithium from the clay-type lithium ore, J. Clean. Prod. 535 (2025) 147130.

[5] R.F. Maritz, R.F. van Schalkwyk, N. Elginöz, G. Akdogan, C. Dorfling, Using life cycle assessment to aid process development for hydrometallurgical recycling of end-of-life lithium ion batteries, Waste Manag. 200 (2025) 114763.

[6] S. Sudarsan, M. Anandkumar, E.A. Trofimov, Survey of diverse hydrometallurgy techniques for recovering and extracting valuable metals from PCB waste: an overview, Int. J. Environ. Sci. Technol. 22 (2) (2025) 1263–1282.

[7] J. Wu, L. Xiao, L. Shen, J.-J. Ran, H. Zhong, Y.-R. Zhu, H. Chen, Recent advancements in hydrometallurgical recycling technologies of spent lithium-ion battery cathode materials, Rare Metals 43 (3) (2024) 879–899.

[8] A. Cornelio, A. Zanoletti, E. Bontempi, Recent progress in pyrometallurgy for the recovery of spent lithium-ion batteries: a review of state-of-the-art developments, Curr. Opin. Green Sustain. Chem. 46 (2024) 100881.

[9] M.D. Cerrillo-Gonzalez, M. Villen-Guzman, C. Vereda-Alonso, J.M. Rodriguez-Maroto, J.M. Paz-Garcia, Towards sustainable Lithium-ion battery recycling: advancements in circular hydrometallurgy, Processes 12 (7) (2024) 1485.

[10] A. Liu, G. Hu, Y. Wu, F. Guo, Life cycle environmental impacts of pyrometallurgical and hydrometallurgical recovery processes for spent lithium-ion batteries: present and future perspectives, Clean Techn. Environ. Policy 26 (2) (2024) 381–400.

[11] E. Rudnik, Innovative approaches to tin recovery from low-grade secondary resources: a focus on (bio)hydrometallurgical and Solvometallurgical methods, Materials 18 (4) (2025) 819.

[12] M.D. Gernon, M. Wu, T. Buszta, P. Janney, Environmental benefits of methanesulfonic acid. Comparative properties and Advantages, Green Chem. 1 (3) (1999) 127–140.

[13] H. Ghaedi, M. Ayoub, S. Sufian, S.M. Hailegiorgis, G. Murshid, S.N. Khan, Thermal stability analysis, experimental conductivity and pH of phosphonium-based deep eutectic solvents and their prediction by a new empirical equation, J. Chem. Thermodyn. 116 (2018) 50–60.

[14] H. Ghaedi, M. Ayoub, S. Sufian, S.M. Hailegiorgis, G. Murshid, S. Farrukh, S. N. Khan, Experimental and prediction of volumetric properties of aqueous solution of (allyltriphenylPhosphonium bromide—Triethylene glycol) deep eutectic solvents, Thermochim. Acta 657 (2017) 123–133.

[15] H. Ghaedi, J. Fu, Y. Liu, Y. Zhang, S.A. Jiskani, A. Raheem, M. Zhao, P.S. Fennell, E. J. Anthony, Iono Non-Hydrothermal (INH) method for synthesis of highly ordered mesoporous silica materials, Chem. Eng. 528 (2025) 172361.

[16] M. Guo, R. Deng, M. Gao, C. Xu, Q. Zhang, Sustainable recovery of metals from e-waste using deep eutectic solvents: advances, challenges, and perspectives, Curr. Opin. Green Sustain. Chem. 47 (2024) 100913.

[17] Y. Zhang, B. Wang, F. Wang, Y. Dai, S. Ren, Y. Hou, W. Wu, A green recyclable process for selective recovery of Li and Fe from spent lithium iron phosphate batteries by synergistic effect of deep eutectic solvent and oxygen, Sep. Purif. Technol. 354 (2025) 128764.

[18] V.E. Huntington, F. Coulon, S.T. Wagland, Assessing metal extraction from metalliferous waste: a study using deep eutectic solvents and chelating agents vs. ethylenediaminetetraacetic acid, J. Environ. Manag. 363 (2024) 121350.

[19] K. Binnemans, P.T. Jones, Methanesulfonic acid (MSA) in clean processes and applications: a tutorial review, Green Chem. 26 (15) (2024) 8583–8614.

[20] K. Binnemans, P.T. Jones, Methanesulfonic acid (MSA) in hydrometallurgy, J. Sustain. Metall. 9 (1) (2023) 26–45.

[21] S. Mishra, P. Ram Jadhao, V. Pandey, K.K. Pant, D. Harbottle, Exploring deep eutectic solvents of methane sulfonic acid and choline chloride: formation, properties, and metal solvent effectiveness, J. Mol. Liq. 415 (2024) 126338.

[22] X. Huang, S. Shi, Y. Wu, G. Xiao, The influence of different anions in ionic liquids on the catalytic hydrolysis of chitin into levulinic acid, J. Mol. Liq. 430 (2025) 127675.

[23] A. Kitada, S. Takeoka, K. Kintsu, K. Fukami, M. Saimura, T. Nagata, M. Katahira, K. Murase, A hydronium solvate ionic liquid: facile synthesis of air-stable ionic liquid with strong Brønsted acidity, J. Electrochem. Soc. 165 (3) (2018) H121.

[24] H. Ghaedi, P. Kalhor, M. Zhao, P.T. Clough, E.J. Anthony, P.S. Fennell, Potassium carbonate-based ternary transition temperature mixture (deep eutectic analogues) for CO2 absorption: characterizations and DFT analysis, Front. Environ. Sci. Eng. 16 (7) (2021) 92.

[25] M.H. Geesi, O. Ouerghi, O. Dehbi, Y. Riadi, Metal-doped TiO2 nanocatalysts in an MX2/urea mixture for the synthesis of benzothiazoles bearing substituted pyrrolidin-2-ones: enhanced catalytic performance and antibacterial activity, J. Environ. Chem. Eng. 9 (4) (2021) 105344.

[26] D. Gangopadhyay, S.K. Singh, P. Sharma, H. Mishra, V.K. Unnikrishnan, B. Singh, R.K. Singh, Spectroscopic and structural study of the newly synthesized heteroligand complex of copper with creatinine and urea, Spectrochim. Acta A Mol. Biomol. Spectrosc. 154 (2016) 200–206.

[27] S. Suzuki, Y. Takeoka, M. Rikukawa, M. Yoshizawa-Fujita, Brønsted acidic ionic liquids for cellulose hydrolysis in an aqueous medium: structural effects on acidity and glucose yield, RSC Adv. 8 (26) (2018) 14623–14632.

[28] A. Zhu, Q. Li, L. Li, J. Wang, One-pot synthesis of 3,4-Dihydro-2(H)-Pyrimidinones catalyzed by reusable acidic choline-based ionic liquids, Catal. Lett. 143 (5) (2013) 463–468.

[29] Y. Wang, X. Gong, Z. Wang, L. Dai, SO3H-functionalized ionic liquids as efficient and recyclable catalysts for the synthesis of pentaerythritol diacetals and diketals, J. Mol. Catal. A Chem. 322 (1) (2010) 7–16.

[30] R. Kore, R. Srivastava, A simple, eco-friendly, and recyclable bi-functional acidic ionic liquid catalysts for Beckmann rearrangement, J. Mol. Catal. A Chem. 376 (2013) 90–97.

[31] A. Wufuer, Y. Wang, L. Dai, Enhanced lignin degradation by a two-step acidic protic bio-based ionic liquid pretreatment method, Biomass Convers, Biorefinery 15 (2021) 29749–29758.

[32] Y. Cui, C. Li, J. Yin, S. Li, Y. Jia, M. Bao, Design, synthesis and properties of acidic deep eutectic solvents based on choline chloride, J. Mol. Liq. 236 (2017) 338–343.

[33] Li4LIFE Project. Available at, https://li4life.eu/, 2025. latest access: 27/12/2025.

[34] Li4LIFE Project, Social Media, LinkedIn, https://www.linkedin.com/company/li4life-eu-project;, 2025. X (formerly Twitter), https://x.com/li4LIFEProject.